AC impedance and state-of-charge analysis of alkaline zinc/manganese dioxide primary cells

S. RODRIGUES[1], N. MUNICHANDRAIAH[2]* and A.K. SHUKLA[1]

[1]*Solid State and Structural Chemistry Unit*
[2]*Department of Inorganic and Physical Chemistry, Indian Institute of Science, Bangalore, 560012, India*
(*author for correspondence, e-mail: muni@ipc.iisc.ernet.in*)

Abstract

Alternating current impedance data of alkaline Zn/MnO$_2$ cells were analysed in view of identification of suitable parameters, which depend on the state-of-charge (SOC) of the cells. The impedance of a slightly discharged cell was found to possess impedance considerably lesser than that of an undischarged cell. The data in the form of Nyquist plot contained an inductance part at very high frequencies, a capacitive semicircle at high frequencies and a diffusion linear spike at low frequencies. The low frequency linear spike gradually transformed into a capacitive semicircle with the decrease of SOC of the cell, which was attributed to the nature of the reactions at the Zn anode. Of several impedance parameters that were examined, equivalent series capacitance (C_s) was found to have a strong dependence on SOC of the alkaline Zn/MnO$_2$ cells. There was a continuous change in a partially discharged cell during its ageing, which was reflected by transformation of low frequency data into a clear semicircle.

1. Introduction

A nondestructive evaluation of state-of-charge (SOC) or depth-of-discharge of primary and secondary batteries by a.c. impedance studies is of interest [1–3]. Prediction of SOC helps in optimum utilization of the battery and in the evaluation of its performance capability. Among the primary batteries, Zn/MnO$_2$ and Mg/MnO$_2$ cells were subjected to a.c. impedance measurements in view of predicting their SOC [4–6]. Alkaline Zn/MnO$_2$ cells have cell-configuration and also performance characteristics different from those of the Leclanché Zn/MnO$_2$ cells [7]. Although some a.c. impedance measurements have been reported [8], there do not appear to be reports on prediction of SOC of alkaline Zn/MnO$_2$ cells using impedance parameters. In the present study, a.c. impedance spectra of commercial alkaline Zn/MnO$_2$ cells were measured at several SOC values and the data were analyzed to identify parameters that showed useful variation with SOC.

2. Experimental details

Commercial 1.75 Ah capacity alkaline Zn/MnO$_2$ cells of AA size (Duracell) were used for the studies. The cells were discharged by passing a constant current of 0.2 A. The value of SOC was taken as 0, when the cell voltage reached 0.8 V during discharge. The electrical circuit consisted of a regulated d.c. power supply, a high resistance and an ammeter in series. The cell voltage and single electrode potentials were measured using a multimeter of high input impedance (Philips, model PP 9007). For the purpose of single electrode studies, a Ag/AgCl, Cl$^-$ reference electrode was introduced through a hole, which was drilled on the outer can of the cell similar to the studies reported in [9]. An agar gel of a saturated solution of KCl was used as the salt bridge. A.c. impedance measurements were carried out using an electrochemical impedance analyser (EG&G PARC, model 6310) and EG&G model 398 software. The a.c. excitation signal was 5 mV at open circuit conditions of the cell and the frequency range was between 100 kHz and 10 mHz. All experiments were carried out in an air-conditioned room at 20 ± 1 °C.

3. Results and discussion

The alkaline Zn/MnO$_2$ cell yields energy density higher than the conventional Leclanché cell, even though the electrode materials are the same. As the name suggests, the electrolyte of the alkaline cell is a concentrated solution of potassium hydroxide, which is immobilized with a gelling agent, commonly sodium carboxymethyl cellulose [7]. The distinction between the two cell

systems exists in the nature of the electrolyte and also in the cell construction. On the one hand, the Zn anode of the Leclanché cell is in the form of a sheet, which also functions as the cell container and the anode current collector. On the other hand, the anode is made of Zn powder placed at the centre and an additional current collector is present in the alkaline cell [10].

3.1. Cell discharge

During discharge of an alkaline Zn/MnO_2 cell, the following reactions take place. At the cathode, the reduction of MnO_2 occurs in two steps:

$$MnO_2 + H_2O + e^- \rightarrow MnOOH + OH^- \qquad (1)$$

$$MnOOH + H_2O + e^- \rightarrow Mn(OH)_2 + OH^- \qquad (2)$$
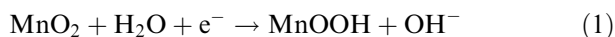
Reaction 1 represents a homogeneous reduction of MnO_2 to MnOOH, and Reaction 2 represents reduction of MnOOH to $Mn(OH)_2$ in a heterogeneous mechanism involving Mn^{3+} ions in the electrolyte. The effectiveness of the second step was reportedly dependent on KOH concentration and current density [7].

At the anode, the oxidation of Zn occurs as

$$Zn \rightarrow Zn^{2+} + 2e^- \qquad (3)$$

Although Zn/Zn^{2+} system is considered to be partially reversible in alkaline media, Zn^{2+} ions are converted into ZnO through a chemical step [7]:

$$Zn^{2+} + 2OH^- \rightarrow ZnO + H_2O \qquad (4)$$
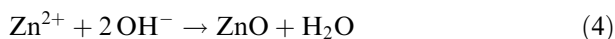
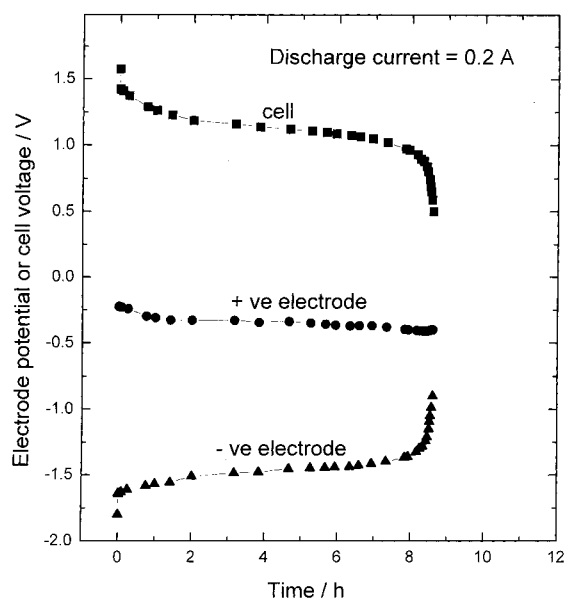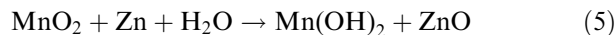Accordingly, the overall cell reaction (addition of Equations 1–4) is

Fig. 1. Galvanostatic discharge curves of an AA size alkaline Zn/MnO_2 cell. Electrode potentials were measured using an Ag/AgCl, Cl$^-$ reference electrode.

$$MnO_2 + Zn + H_2O \rightarrow Mn(OH)_2 + ZnO \qquad (5)$$

An alkaline Zn/MnO_2 cell was discharged at $C/8$ rate and the cell voltage as well as the potentials of individual electrodes were recorded during the course of discharge (Figure 1). The potential of the Zn anode showed a deflection at the end of discharge of the alkaline cell, while the potential of the MnO_2 cathode remained constant. Thus, the capacity of the alkaline cell was limited by the Zn anode.

3.2. Impedance of individual electrodes

A separation of impedance of a sealed cell into contributions of the individual electrodes is rather difficult by nondestructive analysis. To compare the magnitude of impedance of the individual electrodes and the cell, a Ag/AgCl, Cl$^-$ reference electrode was
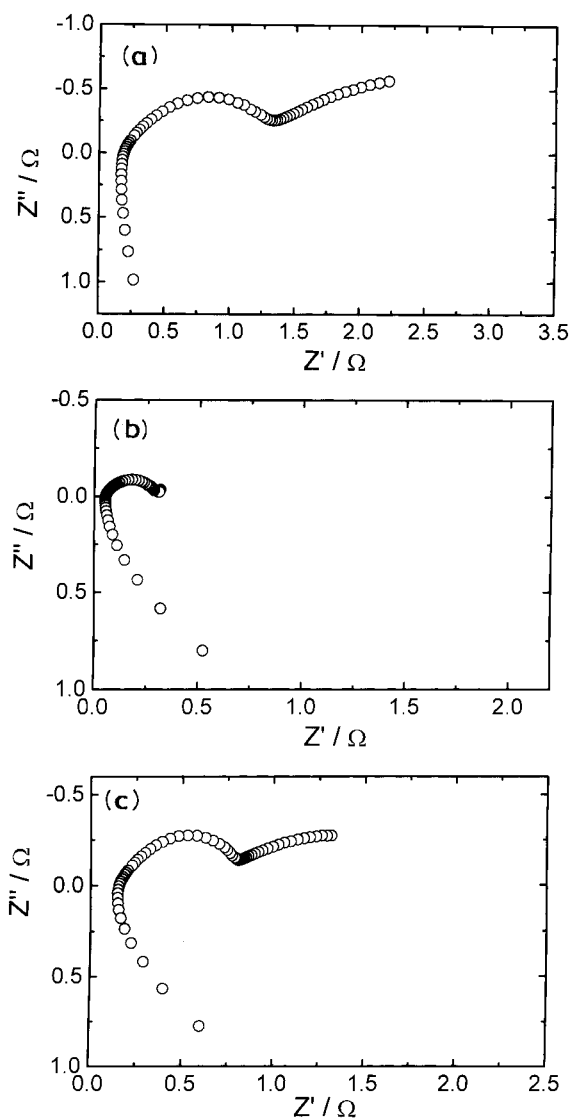
Fig. 2. Nyquist impedance plots of (a) cell, (b) MnO_2 electrode and (c) Zn electrode of an AA size alkaline Zn/MnO_2 cell before discharge in the frequency range from 100 kHz to 10 mHz. Data in (b) and (c) were measured using an Ag/AgCl, Cl$^-$ reference electrode.

introduced into an alkaline cell; the impedances were recorded for the Zn anode, the MnO_2 cathode and the alkaline cell (Figure 2). The magnitude of the impedance of the MnO_2 cathode (Figure 2(b)) was several times smaller than that of either the cell (Figure 2(a)) or the Zn anode (Figure 2(c)). The data, thus, suggested that the cell impedance was dominated by the anode.

3.3. Impedance parameters and SOC

The shape of the Nyquist impedance plot of the alkaline cell (Figure 2(a)) was essentially the same as that reported in the literature [8]. The cell behaviour was inductive for frequencies $(f) > 2.5$ kHz. The semicircle in the frequency range between 2.5 kHz and 12 Hz was due to a parallel combination of charge-transfer resistance (R_{ct}) and double-layer capacitance (C_{dl}); and the linear spike at $f < 12$ Hz was due to a diffusion controlled process. Since the inductive behaviour was attributed to porous nature of the electrodes [1] and also to the electronic contacts to the cell [8], the corresponding high frequency data were not considered for SOC estimation of the cells. The high frequency intercept of the semicircle on the real axis was taken as ohmic

resistance (R_Ω) of the cell, which included the resistance of the electrolyte, separator, current collectors etc. In general, the diameter of the semicircle corresponded to the value of R_{ct}. The value of C_{dl} was calculated, ignoring the constant phase element model, using Equation 6.

$$C_{dl} = \frac{1}{2\pi f' R_{ct}} \tag{6}$$

where f' is frequency corresponding to the maximum value of the imaginary component of the semicircle. The impedance of the alkaline cell was recorded at several SOC values by discharging the cell to the required SOC at the $C/50$ rate and allowing the cell to equilibrate for 2 h at open circuit conditions prior to the measurements. Some of the data are shown in Figure 3 after omitting the inductance data. The impedance of the undischarged cell was high (Figure 2(a)), probably due to passivation of the Zn powder during the storage of the cell between its manufacture and impedance measurements, or due to the organic corrosion inhibitors adsorbed onto the zinc surface [8]. Subsequent to a slight discharge of the cell (i.e., at SOC ~ 0.94), however,
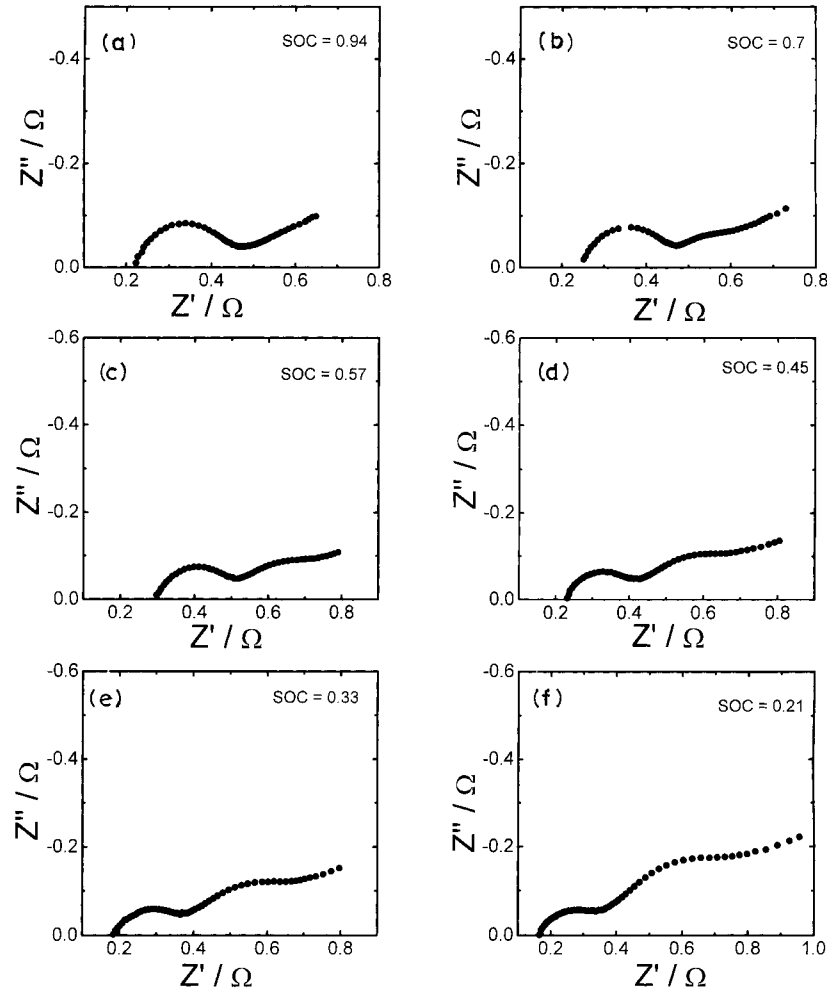

Fig. 3. Nyquist impedance plots of an AA size alkaline Zn/MnO_2 cell at various SOC after omitting inductance data.

the magnitude of the cell impedance decreased considerably (Figure 3(a)). Furthermore, it was found that the low frequency linear spike at high SOC values gradually transformed into an additional semicircle with decrease in SOC. This feature could be explained on the basis of the nature of the electrochemical reaction of Zn. Since the anode was made of Zn powder, the particles were covered with ZnO that was formed in Reaction 4. As the SOC decreased, the proportion of ZnO to Zn increased and at the end of the cell discharge (i.e., SOC ~ 0), the quantity of Zn was negligibly small. The ZnO is a semiconductor. The resistance and capacitance of ZnO are reflected in the form of a semicircle in the low frequency region of the Nyquist impedance plot. Since the proportion of ZnO to Zn increased with decrease in SOC of the cell, there was a gradual appearance and increase in size of the second semicircle (Figure 3). The aspect of second semicircle was further studied by measuring the impedance at several intervals of storing time of a partially discharged cell (cf. Section 3.4).

For the purpose of a qualitative prediction of SOC of the alkaline cell, the appearance of the low frequency semicircle might be considered. Additionally, the following parameters were examined for their variation with SOC: (i) ohmic resistance (R_Ω), (ii) charge-transfer resistance (R_{ct}), (iii) frequency maximum of the high frequency semicircle (f'), (iv) double-layer capacitance (C_{dl}), (v) modulus of impedance ($|Z|$), (vi) phase angle (ϕ), (vii) real part (Z') and (viii) imaginary part (Z'') (Figures 4 and 5). In view of the overall cell reaction (Equation 5), a change in the electrolyte conductivity was expected as there was a decrease in the H_2O content with decrease of SOC. By contrast, the parameter R_Ω, which reflected the electrolyte resistance, was nearly invariant with SOC, although there was some scatter (Figure 4(a)). Since the electrolyte was a concentrated alkali and also the electronic resistances of the electrode material varied with cell discharge, the effect of H_2O consumption in Reaction 5 did not clearly reflect in the variation of R_Ω. Although there was no scatter in R_{ct} (Figure 4(b)), it was invariant during the cell discharge, except in the case of the undischarged cell (not shown in Figure 4(b), but was evident from Figure 2(a)) and also at the end of the cell discharge, where the values of R_{ct} were much higher. Consequently both R_Ω and R_{ct} were not useful for prediction of SOC of the alkaline Zn/MnO$_2$ cells. In the case of f', it was nearly constant at SOC values between 1.0 and 0.5 (Figure 4(c)). However, it decreased linearly from about 150 Hz at SOC ~ 0.5 to 12 Hz at SOC ~ 0.1. Thus, f' could be a useful parameter for predicting SOC of the alkaline cell in lower SOC range. Double-layer capacitance (C_{dl}) increased from about 4 mF at SOC ~ 0.4 to 18 mF at SOC ~ 0, while it was constant at SOC > 0.4 (Figure 4(d)). Although the increase of values between 0.4 and 0 was not linear, C_{dl} could be useful to some extent for prediction of SOC of the cells.

An examination of Figure 5 suggested that the parameters Z', Z'' and $|Z|$ showed a pronounced increase at
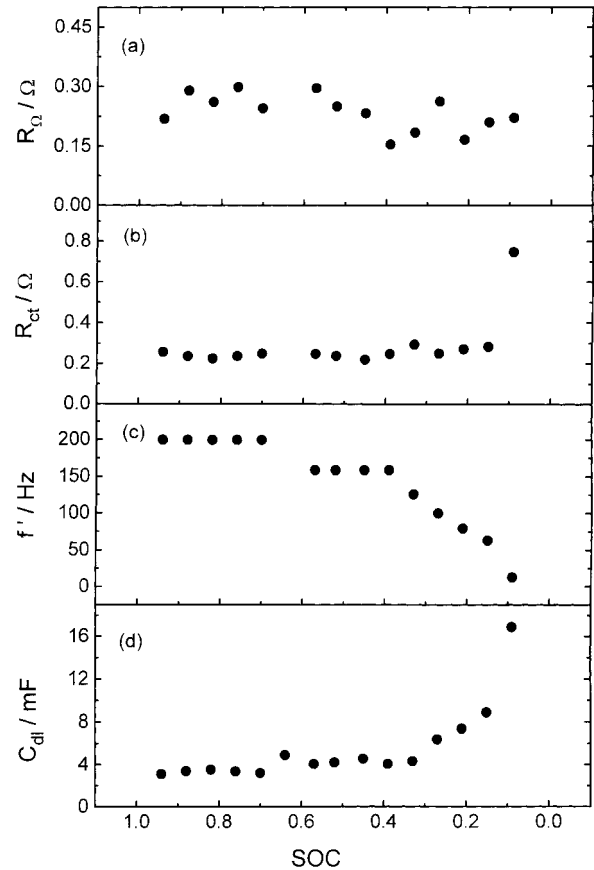

Fig. 4. Variation of impedance parameters: (a) ohmic resistance (R_Ω), (b) charge-transfer resistance (R_{ct}), (c) frequency maximum (f'), and (d) double-layer capacitance (C_{dl}) with SOC of an AA size alkaline Zn/MnO$_2$ cell.

low frequencies with a decrease of SOC between 0.3 and 0 (Figure 5(a)–(c)). At SOC > 0.3, however, there was a negligibly small variation in their values. In the case of ϕ, the variation at several frequencies was irregular (Figure 5(d)). These parameters were thus found to have limited use for prediction of SOC of the alkaline cells. The possibility of prediction of SOC of the alkaline cells was further examined by considering equivalent series resistance (R_s) and equivalent series capacitance (C_s). For this purpose, charge-transfer resistance (R_{ct}) and the parallel double-layer capacitance (C_{dl}) were transformed into equivalent R_s and C_s using Equations 7 and 8 [11]:

$$R_s = R_{ct}/(1 + (\omega R_{ct}C_{dl})^2) \tag{7}$$

$$C_s = C_{dl}/(1 + 1/(\omega R_{ct}C_{dl})^2) \tag{8}$$

The values of R_s and C_s calculated for several frequencies between 100 and 10 mHz are shown in Figure 6. On the one hand, the value of R_s was nearly the same at all frequencies and it was invariant with SOC except at SOC ~ 0, where it was very high (Figure 6(a)). On the other hand, there was a linear variation in the value of C_s throughout the SOC range of alkaline cell (Figure 6(b)). The variation was significant at low frequencies in particular. At 10 mHz, for example, there
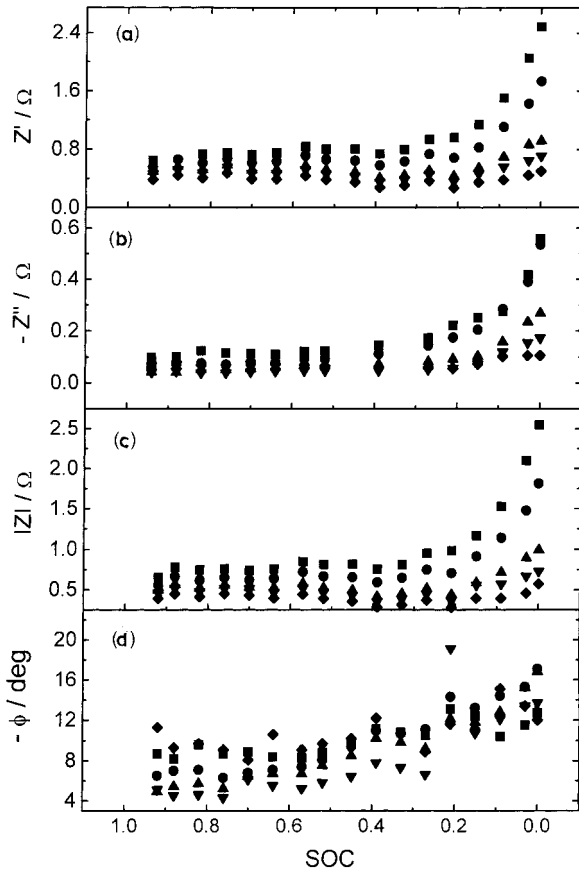
Fig. 5. Variation of Z', Z'', $|Z|$ and ϕ with SOC of an AA size alkaline Zn/MnO$_2$ cell at 0.01(■), 0.1 (●), 1.585 (▲), 10 (▼) and 100 Hz (◆).

Fig. 6. Variation of (a) equivalent series resistance (R_s) and (b) equivalent series capacitance (C_s) with SOC of an AA size alkaline Zn/MnO$_2$ cell at 10 (1), 25 (2), 50 (3) and 100 mHz (4).

was a decrease in the value of C_s from about 1.3×10^5 F at SOC ~ 0.9 to 0.26×10^5 F at SOC ~ 0.09. Thus, C_s was found to be a useful parameter for prediction of SOC of alkaline Zn/MnO$_2$ cells, akin to the studies reported on Ni–Cd [12], Pb-acid [13] and lithium-ion cells [14].

3.4. Impedance of the partially discharged cell during ageing

A cell was discharged to SOC ~ 0.5 and its impedance data were recorded at several intervals of storing at $20 \pm 1\,^\circ\text{C}$. Some of the data in the Nyquist form are shown in Figure 7 after omitting the inductance data. It was found that the nature of the high frequency semicircle was nearly invariant with ageing of the partially discharged cell. On the other hand, the low frequency data underwent considerable variation. The low frequency data appeared as a hump when measured 24 h after discharging to SOC ~ 0.5 (Figure 7(a)). On ageing, the hump gradually grew into a semicircle as seen in Figure 7(b)–(f). The following possibilities could be considered for a gradual growth of the low frequency semicircle. (a) It is known that the electrode reaction of Zn in alkaline medium is partially reversible [6]. That means, Zn metal partially undergoes corrosion although the alkaline electrolyte contains Zn^{2+} ions owing to saturation with ZnO. Thus, the following partial reac-
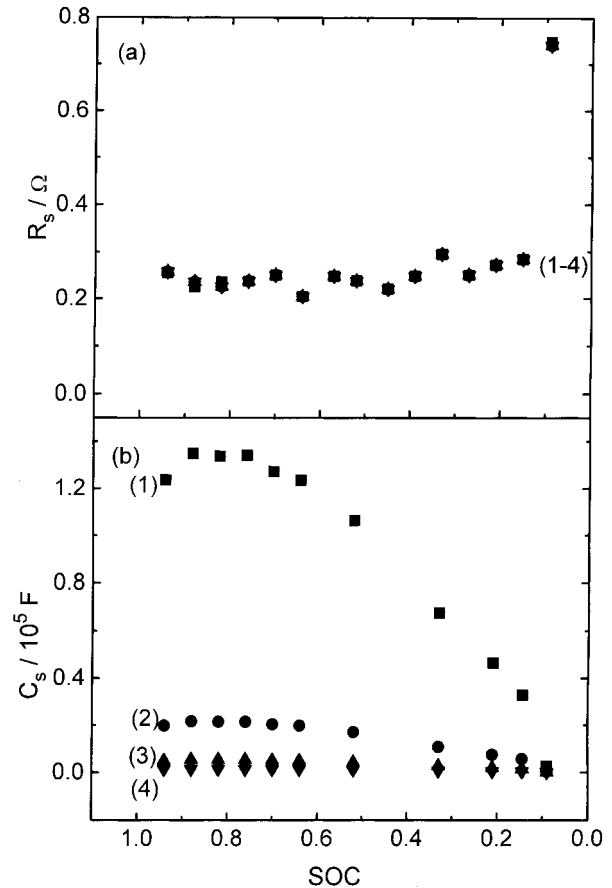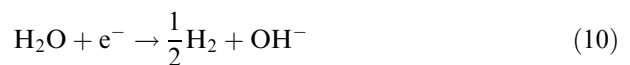
tions are possible at the Zn anode/electrolyte interface under open circuit conditions:

$$Zn \rightarrow Zn^{2+} + 2\,e^- \qquad (3)$$

$$Zn^{2+} + 2\,e^- \rightarrow Zn \qquad (9)$$

$$H_2O + e^- \rightarrow \frac{1}{2}H_2 + OH^- \qquad (10)$$

Reactions 3 and 9 together constitute the partial reversible process, whereas Reactions 3 and 10 together represent the partial corrosion process under open circuit conditions. Both these processes, however, are affected by the presence of surface film of ZnO on the Zn anode particles. While the high frequency semicircle could be attributed to the partial reversible process, the low frequency semicircle could be due to the corrosion processes. The gradual transformation of the low frequency data into a clear semicircle could be attributed to the changes that occur at Zn/electrolyte interface. The corrosion rate of the Zn decreased on ageing of the cell under open-circuit conditions. This was due to an increased coverage of ZnO film on the Zn surface, thus, reducing the effective area of film-free Zn surface. (b) An alternative explanation for the appearance of the
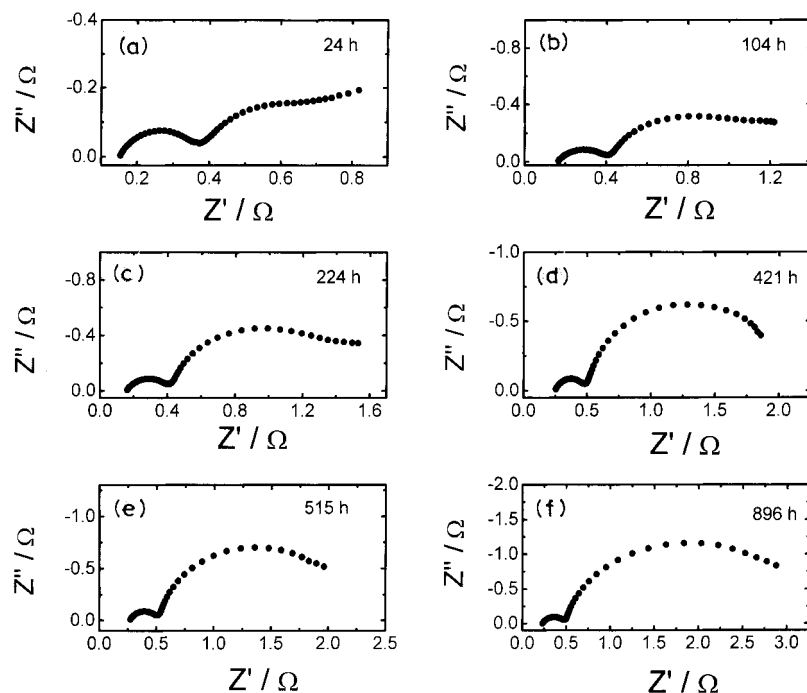
Fig. 7. Nyquist impedance plots of an AA size alkaline Zn/MnO$_2$ cell during ageing subsequent to discharge to SOC $\sim$0.5. Corresponding ageing time is indicated.

additional semicircle was that the surface film of ZnO possessed resistance as well as its parallel capacitance (cf. Section 3.3). Thus, one of the semicircles was due to a parallel R_{ct} and C_{dl}, and the other semicircle was due to a parallel surface ZnO film resistance and its capacitance. The relative positions of the two semicircles depended on the corresponding (RC) time constant values. (c) Another possibility was that the molecules of corrosion inhibitors and gelling agents such as sodium carboxymethylcellulose usually added into the electrolyte were adsorbed on the surface of Zn. The adsorbed layer of the inhibitor owing to its parallel resistance and capacitance could be responsible for the appearance of the second semicircle. Although it is not certain at the present time, which of the possibilities was really responsible for the appearance of the second semicircle, it is clear that some changes continuously occur in a partially discharged alkaline cell during its open-circuit ageing period.

Attempts were made to fit the impedance data by a Boukamp equivalent circuit program, which employed a nonlinear least square fitting procedure. Since the circuit description code of the program did not allow the Randle's equivalent circuit model consisting of a Warburg element, the experimental data, consisting of low frequency linear spikes, could not be fitted. The data consisting of two clear semicircles, however, could be fitted successfully. The capacitances were replaced by constant phase elements, similarly to previous work [14, 15]. A typical impedance spectrum containing the experimental data and the theoretical curves generated
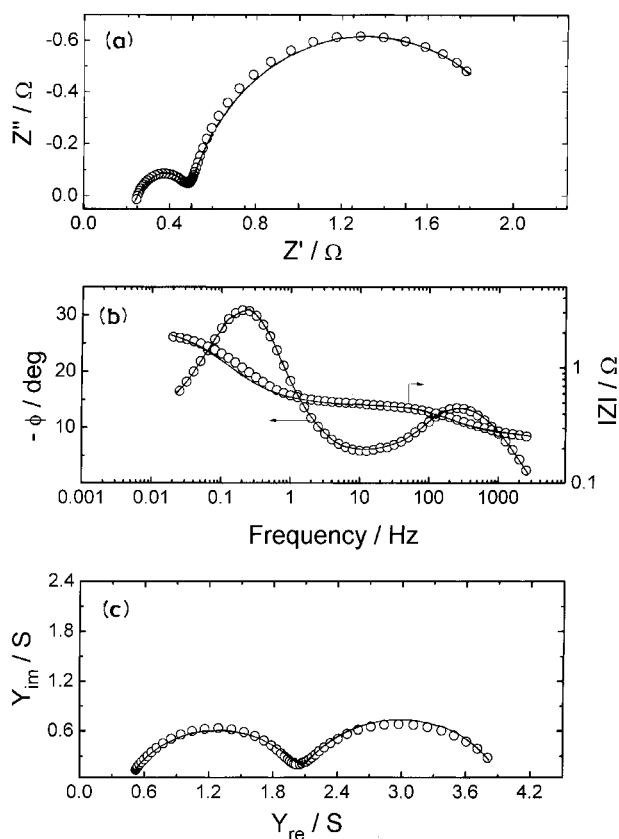

Fig. 8. Electrochemical impedance spectrum in (a) Nyquist, (b) Bode and (c) admittance forms of an AA size alkaline Zn/MnO$_2$ cell at 421 h after discharging to SOC $\sim$0.5. Experimental data are shown by symbols and theoretical curves obtained from NLLS fit results are shown by solid curves.
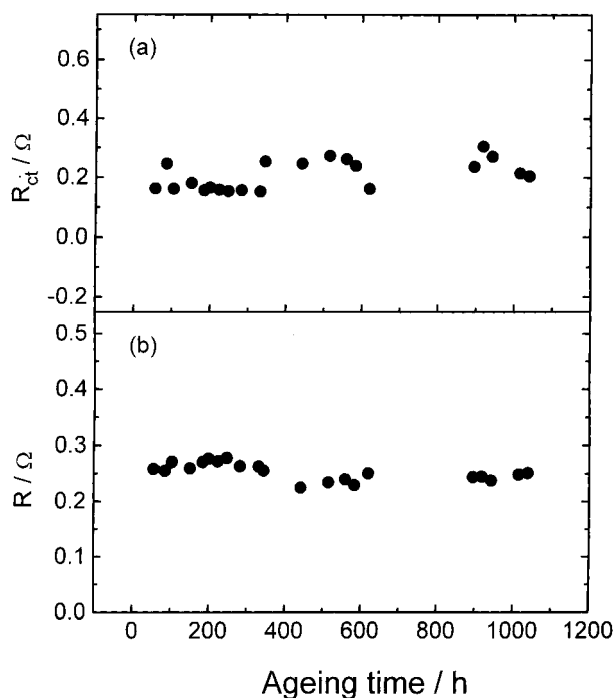
Fig. 9. Variation of (a) charge-transfer resistance (R_{ct}) corresponding to the high frequency semicircle and (b) resistance (R) corresponding to the low frequency semicircle of an AA size alkaline Zn/MnO_2 cell with ageing time subsequent to its discharge to SOC ~ 0.5.

using the fitted results are shown in Figure 8 in different forms. Superimposing of the experimental data points and the theoretical curves suggested that the fitting procedure was reasonably correct. The resistances corresponding to the two semicircles are shown in Figure 9 as a function of ageing time subsequent to the cell discharge to SOC ~ 0.5. It was found that these two parameters were nearly invariant with ageing time, although there were significant changes in the nature of the impedance data.

4. Conclusions

The impedance of a slightly discharged cell was much less than the undischarged cell. The data in the Nyquist form contained an inductance part at very high frequencies, a capacitive semicircle at high frequencies and a linear spike at low frequencies. The linear spike gradually transformed into a capacitive semicircle with a decrease in SOC of the cell. Among various impedance parameters, equivalent series capacitance (C_s) was found to have a strong dependence on SOC of the cells. There was a continuous change in the partially discharged cell during its ageing, which was reflected in transformation of low frequency data into a clear semicircle.

References

1. N.A. Hampson, S.A.G.R. Karunathilaka and R. Leek, *J. Appl. Electrochem.* **10** (1980) 3.
2. F. Huet, *J. Power Sources* **70** (1998) 59.
3. S. Rodrigues, N. Munichandraiah and A.K. Shukla, *J. Power Sources* (1999), in press.
4. M.L. Gopikanth and S. Sathyanarayana, *J. Appl. Electrochem.* **9** (1979) 581.
5. S.A.G.R. Karunathilaka, N.A. Hampson, R. Leek and T.J. Sinclair, *J. Appl. Electrochem.* **10** (1980) 799.
6. N. Munichandraiah, *J. Appl. Electrochem.* **29** (1999) 463.
7. N.C. Cahoon and H.W. Holland, 'The Primary Batteries', Vol. 1, edited by G.W. Heise and N.C. Cahoon (J. Wiley & Son, New York, 1971), p. 239.
8. M.J. Root, *J. Appl. Electrochem.* **25** (1995) 1057.
9. R. Barnard, L.M. Baugh and C.F. Randell, *J. Appl. Electrochem.* **17** (1987) 165.
10. R.F. Scarr and J.C. Hunter, 'Handbook of Batteries', edited by D. Linden (McGraw-Hill, New York, 2nd edn, 1994), p. 10.1.
11. S. Sathyanarayana, S. Venugopalan and M.L. Gopikanth, *J. Appl. Electrochem.* **9** (1979) 125.
12. V.V. Viswanathan, A.J. Salkind, J.J. Kelley and J.B. Ockerman, *J. Appl. Electrochem.* **25** (1995) 716.
13. V.V. Viswanathan, A.J. Salkind, J.J. Kelley and J.B. Ockerman, *J. Appl. Electrochem.* **25** (1995) 729.
14. S. Rodrigues, N. Munichandraiah and A.K. Shukla, *J. Solid State Electrochem.* **3** (1999) 397.
15. N. Munichandraiah, L.G. Scanlon and R.A. Marsh, *J. Power Sources* **72** (1998) 203.